ASTR 565
Computer Problem 3: Convection and Radiation Zones in Main Sequence Stars

Laurel Farris

03 November 2015

1 Introduction

Energy is transferred through the interior of stars by means of three primary mechanisms: radiation, conduction, and convection. The efficiency of this transfer depends on the temperature gradient, one of the fundamental equations of stellar structure. Convection arises due to instabilites in stellar interiors; if a parcel of gas is displaced and its mass density is less than that of its surroundings, the blob will continue to rise, and this is convection.

If the pressure balance between the blob and its surroundings adjusts itself on much shorter timescales than the temperature (due to acoustic waves traveling through this region), the displacements are adiabatic.

While convection is not well understood, there are several constraints that can be place on when and where this phenomenon occurs in a range of stellar masses. One of these is ∇, defined as

$$\nabla \equiv \frac{dlnT}{dlnP} = -\frac{r^2 P}{Gm\rho}\frac{1}{T}\frac{dT}{dr} \tag{1}$$

This is the true driving gradient of the star, and is determined by the mechanism that is driving the luminosity to escape. If this mechanism happened to be radiative transport only, then ∇ would be equal to the radiative gradient, ∇_{rad}, defined as

$$\nabla_{rad} \equiv \left(\frac{dlnT}{dlnP}\right)_{rad} = -\frac{3}{16\pi acG}\frac{P\kappa_R}{T^4}\frac{L}{m} \tag{2}$$

This gradient is required for a purely radiative region. If ∇_{rad} is greater than ∇, then ∇ is not steep enough to transport the energy and an additional mechanism is required to drive the radiation outward.

This leads us to the third gradient, the adiabatic gradient, ∇_{ad}, defined as

$$\nabla_{ad} \equiv \left(\frac{dlnT}{dlnP}\right)_{ad} = \frac{\Gamma_2 - 1}{\Gamma_2} \tag{3}$$

The condition for instability is the **Schwarzschild criterion**: $\nabla > \nabla_{ad}$; if the temperature gradient is not steep enough to carry luminosity through radiative transport, convection is required to do so.

Another way to model convection is through the Brunt-Väisälä frequency (N^2):

$$N^2 = g\Big(\frac{1}{\gamma P}\frac{dP}{dr} - \frac{1}{\rho}\frac{d\rho}{dr}\Big) \tag{4}$$

or, in terms of the temperature gradients:

$$N^2 = \frac{g^2\rho}{P}(\nabla_{ad} - \nabla + \nabla_\mu) \tag{5}$$

where ∇_μ is the composition gradient. Temporarily ignoring ∇_μ (which is effectively zero in convective regions; the mixing of materials results in a constant mean molecular weight), one can see that N^2 will be negative when the criteria for instability holds ($\nabla > \nabla_{ad}$), indicating convection. However, it is possible for ∇_μ to be large enough to cause N^2 to be positive, resulting in a medium that is stable, even though it satisfies the Schwarzschild criterion. When this happends, the region satisfies the *Ledoux criterion*, resulting in *semiconvection*, or weak convection. Physically, blobs of material are subject to oscillation about a point in their static environment, but are stable to large-scale convection.

2 Methods

To explore the variation in location and depth of convection zones for main sequence stars, MESA was used to produce models for 19 stars with initial masses ranging from 1.3 $M_\odot$ to 20 $M_\odot$. An HR diagram showing the final stage for each model (where the hydrogen mass fraction dropped to 0.35) is shown in figure 1.

Each of the gradients described in the introduction is available as output in MESA, as well as the Brunt-Väisälä frequency, so these values were used to determine where the convection boundaries might be for each model. Since the criteria for instability ($\nabla > \nabla_{ad}$) can be met and still only result in a region that is semi-convective, as discussed above, the sign of the Brunt-Väisälä frequency (negative) was used to determine where large scale convection was taking place. The results of these data for each model are shown in figures 2 and 3, where figure 2 shows the convective boundaries as a function of mass ratio, and figure 3 shows the convective boundaries as a function of radius. Once the endpoints of region were found, a cubic interpolation was applied to make these boundaries continuous across all masses between 0.3 $M_\odot$ and 20 $M_\odot$.

Also shown in the figures is where the dominant nuclear burning process (proton-proton chain or CNO cycle) is taking place in the non-convective interiors. Both processes were also contained in output variables from MESA (pp and cno), but determining the location where each one takes place was not as straight-forward as simply using the sign of the numbers. If the ratio of cno to pp was greater than 1, the CNO cycle was assumed to be the dominant reaction taking place. However, the pp values were always greater than zero (though not always by much, as they could get as low as $\sim 10^{-30}$). The values did increase substantially around 1.0, so anything greater than this was determined to be a dominant process.

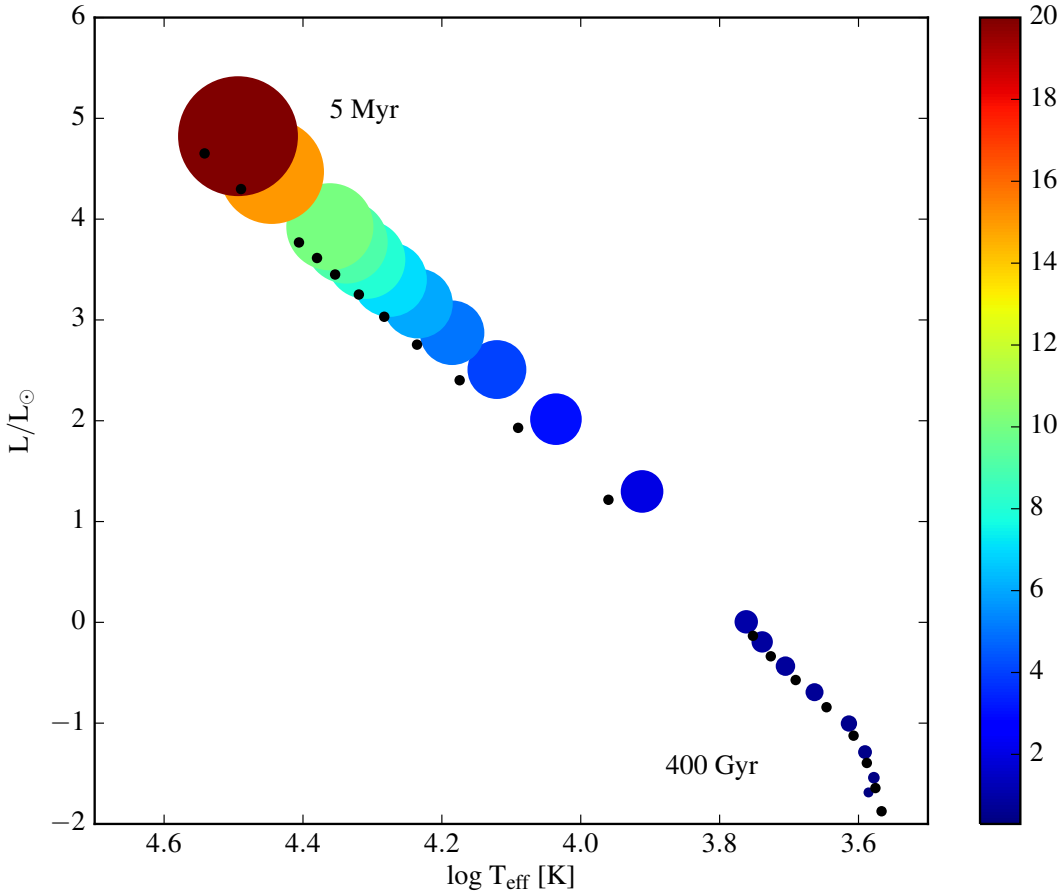

Figure 1: HR-Diagram of all models at both the ZAMS (black dots) and their final positions upon reaching a hydrogen mass fraction of 0.35. The final radius of each star is plotted to scale by size, and the color is an indication of the final mass (in units of $M_\odot$). The final age is displayed for highest (20 $M_\odot$) and lowest (0.3 $M_\odot$) mass stars for comparison. The ZAMS points are not scaled.

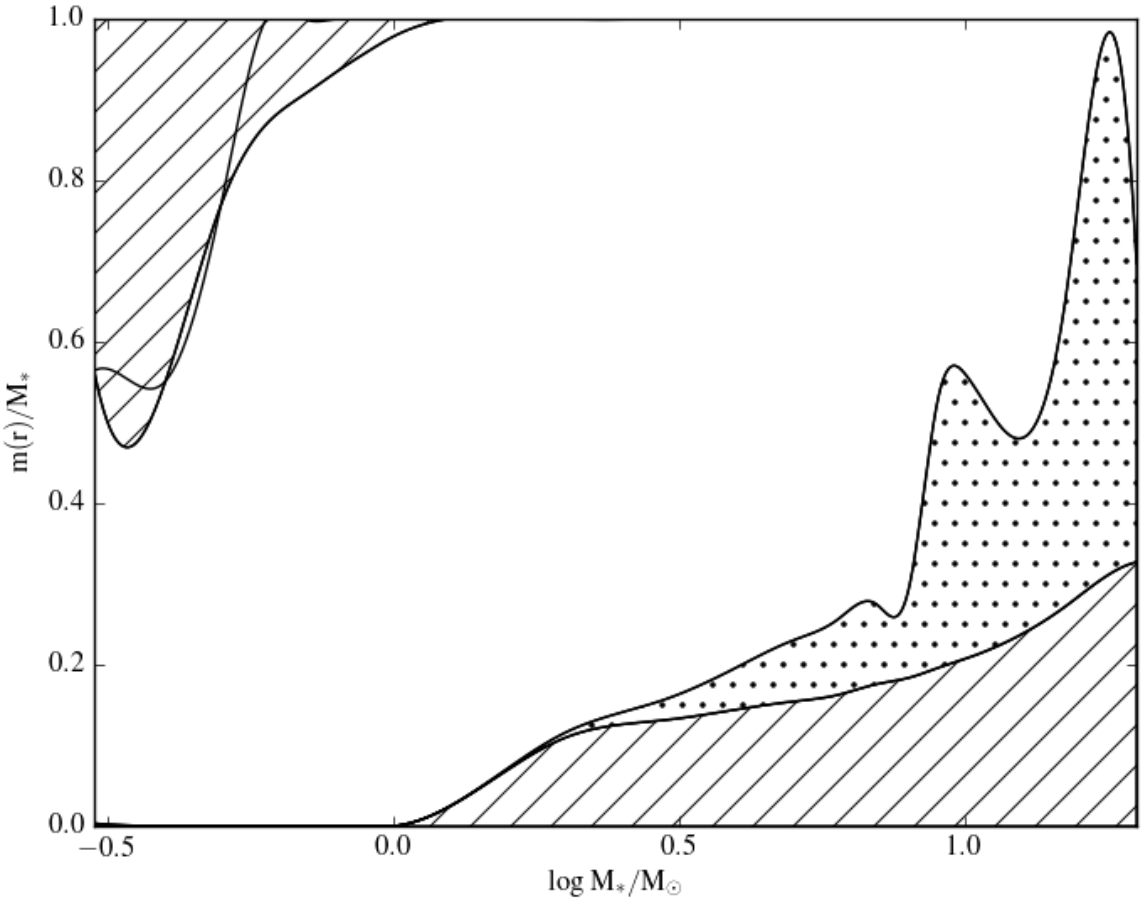

Figure 2: This plot shows where the convection zone boundaries of each model occur according to the mass fraction of the entire star. The hatched areas show the location of the convection zones, the dotted areas are where the CNO cycle is taking place, and the other areas are where the proton-proton chain is taking place.

For further analysis, the gradients for the 0.3 $M_\odot$ star and the 10 $M_\odot$ were plotted as functions of temperature, as a comparison between convective behavior in low and high mass stars. The results are shown in figures 4 and 5. For these same two models, the Brunt-Väisälä frequency was also plotted as a function of temperature to examine areas of semi-convection. These results are shown in figures 6 and 7.

3 Results

The first thing that is immediately apparent upon examination of figures 2 and 3, is that the variation of convective boundaries with stellar mass across the range of models is much different than the variation with stellar radius. Low mass stars are known to be fully convective due to larger opacities, so we would expect figure 3 to show convection throughout the majority of the radius (unfortunately, due to an unknown programming error, the plot does not follow the correct trend for low mass stars).

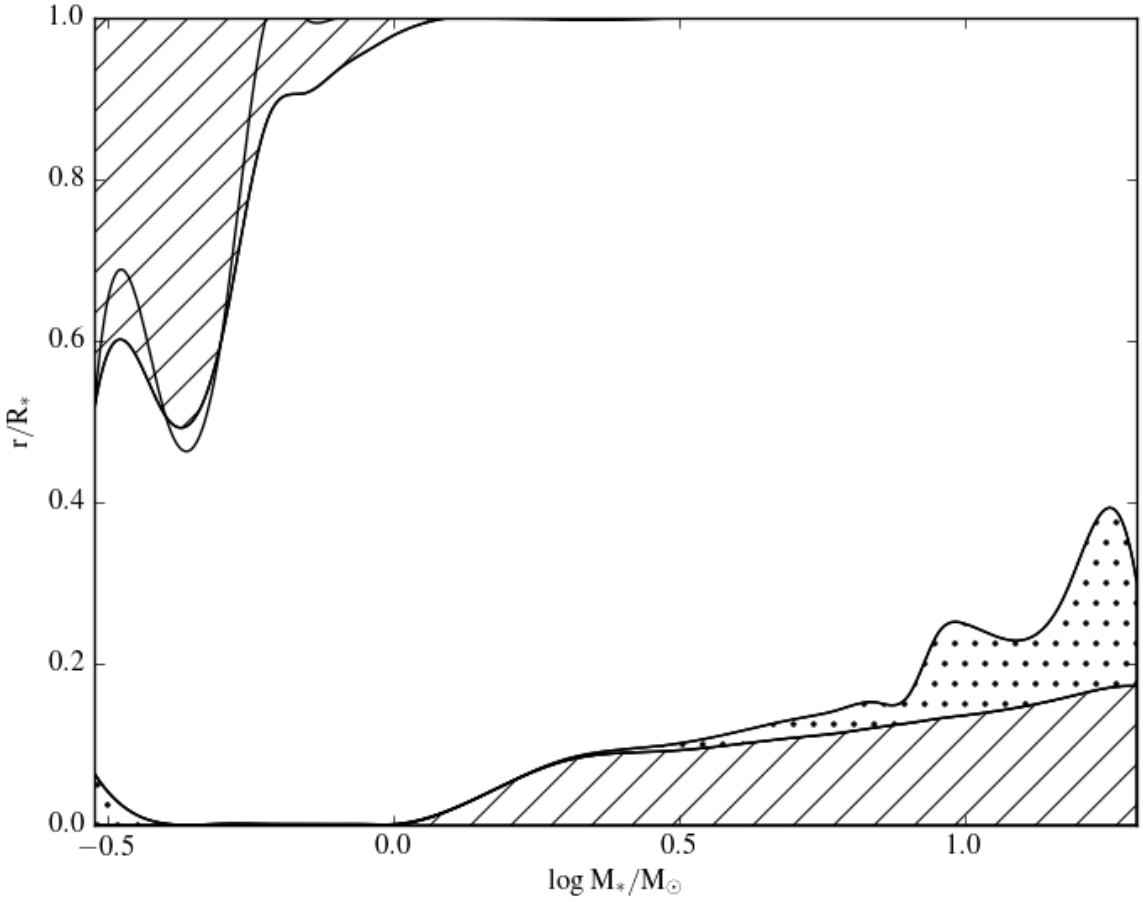

Figure 3: This is the same as figure 2, but with the boundaries shown according to their radial value (as a fraction of each star's total radius).

The low mass model can be further explained in figure 4, where the radiative gradient for the 0.3 $M_\odot$ model is much higher than the adiabatic and true gradients. As discussed above, this implies that the true driving gradient of the star is not steep enough to transport the luminosity by radiation alone. This only ceases to be the case in the hottest region of the star, where ∇_{rad} briefly drops below the other two. This corresponds to where the Brunt-Väisälä frequency is positive for this model, as shown in figure 6.

For the higher mass models (greater than or equal to $1M_\odot$), a convective core appears to emerge in figures 2 and refmoney2, as we would expect. Convection in the outer regions extends to shallower depths as the temperature increases, and as can also be seen in the figures , the outer convection region practically disappears at the surface. Contrary to the gradients for the 0.3 $M_\odot$ model, the radiative gradient for the 10 $M_\odot$ model (figure 5) is lower than the adiabatic, except in the deepest regions, where core convection takes place for high mass stars, and a few places closer to the surface. Between these two regions is where the Brunt-Väisälä has positive values, as shown in figure 7. The spikes at the edges occur near the boundaries of the convection zones discussed above, and the inner region of the high-mass model shows varying degrees of semi-convection.

To obtain a more quantitative idea of why convection takes place where it does (particularly for the 0.3 $M_\odot$ and 10 $M_\odot$ models as investigated here, equation (2) can be rewritten as

$$\nabla_{rad} = \frac{3k_B}{16\pi acGm_u}\frac{\kappa}{\mu}\frac{L}{m}\frac{\rho}{T^3} \tag{6}$$

where it is easier to see that a high value of ∇_{rad} can arise from $\frac{L}{m}$, κ, and/or ρ/T^3 being large. The opacity (κ) is definitely larger for lower mass stars, where their surface temperatures are cooler, and thus ρ/T^3 can also get quite large.

4 Conclusions

Low mass stars tend to have high opacities in their outer regions, which can lead to convection, whereas high mass stars have a high energy generation rate, leading to convection in their cores. This is illustrated plainly in figures 2 and 3, but doesn't explain the small convection areas in the outermost regions of the high mass stars. In figure 5, the different between ∇_{ad} and ∇_{rad} oscillates back and forth a couple times, illustrating the convective inconsistency in the lower temperature regions (outer layers). The Brunt-Väisälä frequency for the 0.3 $M_\odot$ star has a positive value between temperatures of about 4.5 MK and 9 MK. The slope of the line is fairly smooth, except for two significant spikes around temperatures of 7.5 MK and a smaller one at 6.3 MK. Since the ratio ρ/T^3 can result in convection if it gets large enough, this may suggest a low enough density at those temperatures for partial displacement of material, but not low enough to become completely unstable.

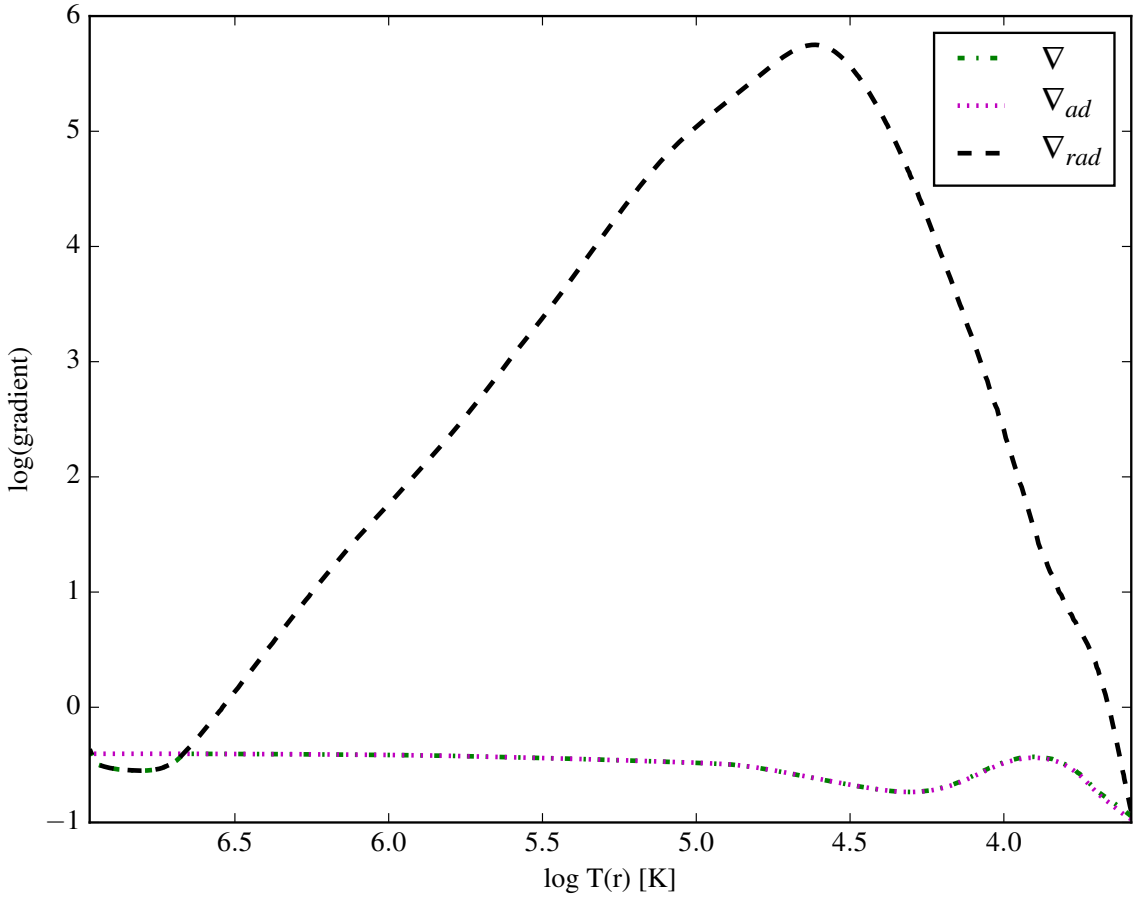

Figure 4: This plot shows the temperature gradient (∇), the adiabatic gradient (∇_{ad}), and the radiative gradient (∇_{rad}) for a 0.3 $M_\odot$ model as functions of (decreasing) temperature.

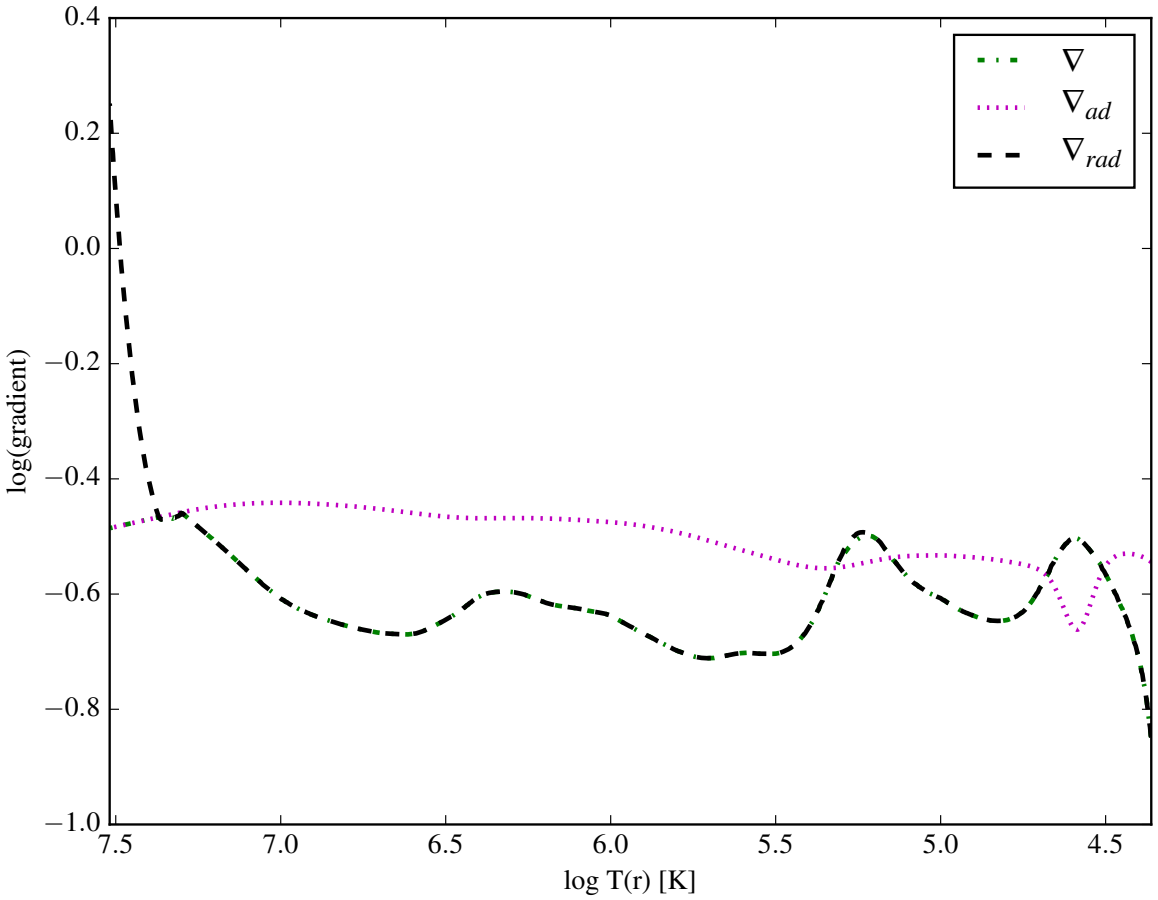

Figure 5: This plot shows the temperature gradient (∇), the adiabatic gradient (∇_{ad}), and the radiative gradient (∇_{rad}) for a 10 $M_\odot$ model as functions of (decreasing) temperature.

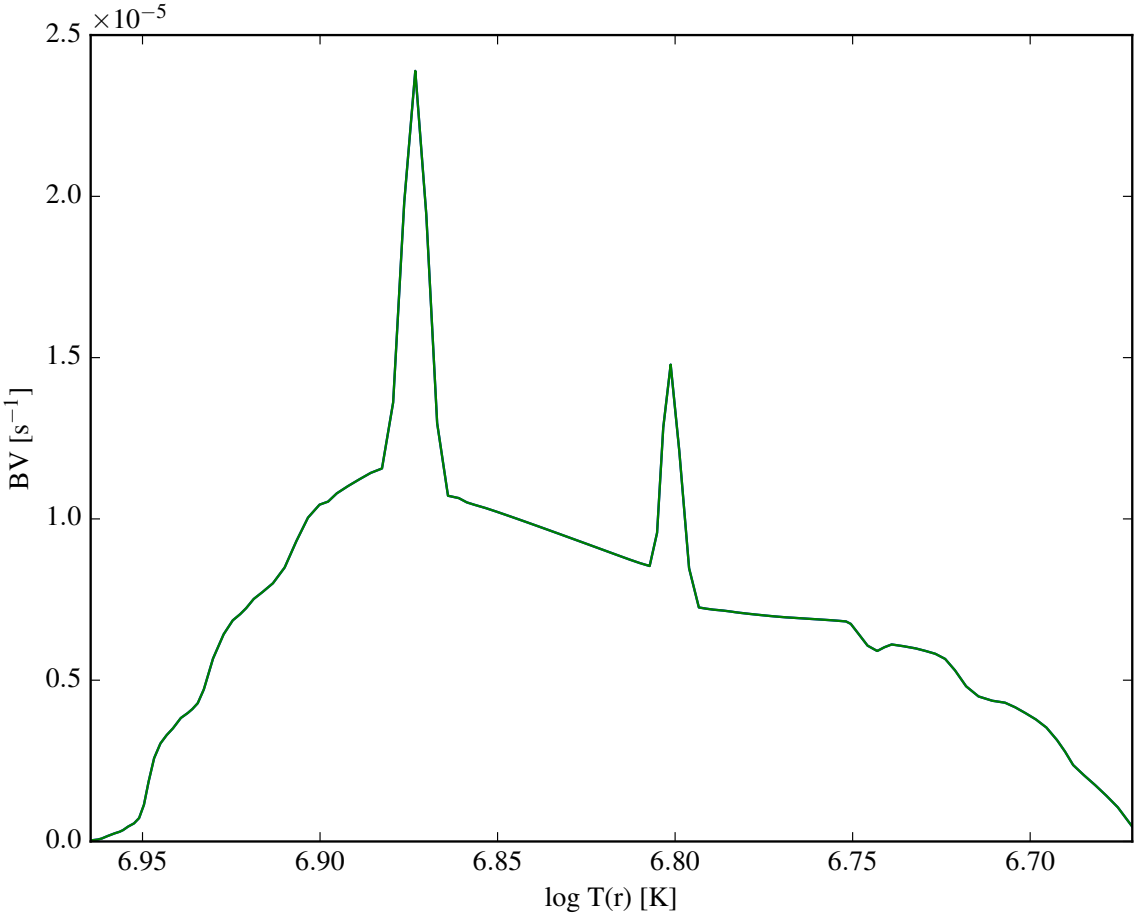

Figure 6: This plot shows the Brunt-Väisälä frequency (N^2) for a 0.3 $M_\odot$ model as a function of (decreasing) temperature.

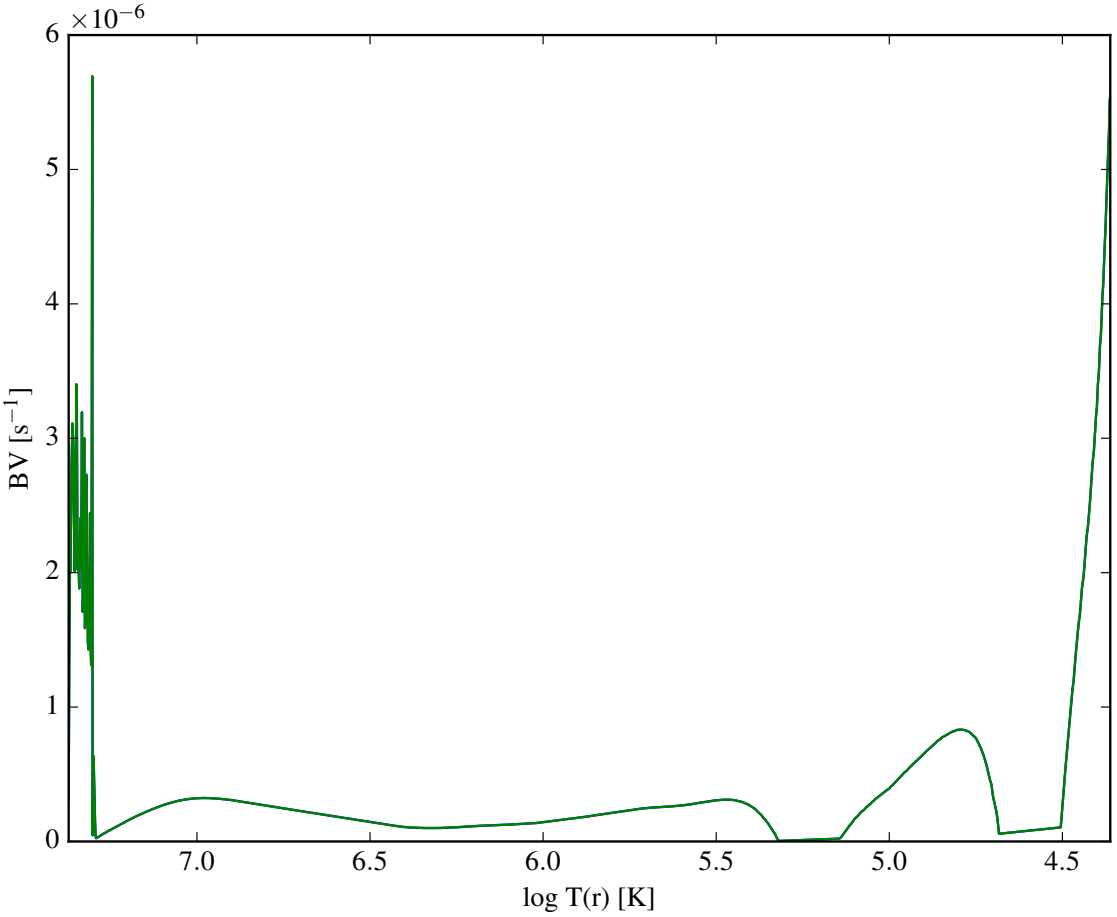

Figure 7: This plot shows the Brunt-Väisälä frequency (N^2) for a 10 $M_\odot$ model as a function of (decreasing) temperature.